Importance of Many-Body Effects in the Kernel of Hemoglobin for Ligand Binding

Cédric Weber, David D. O'Regan, Nicholas D. M. Hine, Peter B. Littlewood, Gabriel Kotliar, and Mike C. Payne

Phys. Rev. Lett. **110**, 106402 — Published 6 March 2013

DOI: 10.1103/PhysRevLett.110.106402

Importance of many body effects in the kernel of hemoglobin for ligand binding

Cédric Weber,[1,2] David D. O'Regan,[2,3] Nicholas D. M. Hine,[2,4]
Peter B. Littlewood,[2,5] Gabriel Kotliar,[6] and Mike C. Payne[2]

[1]*King's College London, Theory and Simulation of Condensed Matter (TSCM), The Strand, London WC2R 2LS*
[2]*Cavendish Laboratory, J. J. Thomson Av., Cambridge CB3 0HE, U.K.*
[3]*Theory and Simulation of Materials, École Polytechnique Fédérale de Lausanne, Station 12, 1015 Lausanne, Switzerland*
[4]*Department of Materials, Imperial College London, Exhibition Road, London SW7 2AZ, U.K.*
[5]*Physical Sciences and Engineering, Argonne National Laboratory, Argonne, Illinois 60439, U.S.A.*
[6]*Rutgers University, 136 Frelinghuysen Road, Piscataway, NJ, U.S.A.*

We propose a mechanism for binding of diatomic ligands to heme based on a dynamical orbital selection process. This scenario may be described as *bonding determined by local valence fluctuations*. We support this model using linear-scaling first-principles calculations, in combination with dynamical mean-field theory, applied to heme, the kernel of the hemoglobin metalloprotein central to human respiration. We find that variations in Hund's exchange coupling induce a reduction of the iron 3*d* density, with a concomitant increase of valence fluctuations. We discuss the comparison between our computed optical absorption spectra and experimental data, our picture accounting for the observation of optical transitions in the infrared regime, and how the Hund's coupling reduces, by a factor of five, the strong imbalance in the binding energies of heme with CO and O_2 ligands.

Metalloporphyrin systems, such as heme, play a central role in biochemistry. The ability of such molecules to reversibly bind small ligands is of great interest, particularly in the case of heme which binds diatomic ligands such as oxygen and carbon monoxide. Heme acts as a transport molecule for oxygen in human respiration, while carbon monoxide inhibits this function. Despite intensive studies [1–3], the binding of the iron atom at centre of the heme molecule to O_2 and CO ligands remains poorly understood. In particular, one problem obtained with density functional theory [4] (DFT) approaches to ligand binding of heme is that the difference in the binding energy ($\Delta\Delta E$) of carboxy-heme and oxy-heme is very large, and the theory predicts an unrealistic binding affinity to CO, several orders of magnitude larger than to O_2 [5, 6].

Recent progress has been made to cure this problem using DFT+U for the molecular systems [7, 8], with which it was found that the inclusion of many body effects in the calculations reduced the imbalance between O_2 and CO affinities [9]. Inclusion of conformal modifications, such as the Fe-C-O binding angle [10], or the deviation of the Fe atom from the porphyrin plane, were also shown to affect CO and O_2 binding energies.

A general problem encountered by DFT is the strong dependence of the energetics and the spin state on small changes in the geometry. In particular, traditional DFT fails to describe the correct high-spin ground state of heme molecules. DFT+U provides an improved description [7, 11], but is known to overestimate magnetic moments and gives often artificial and non physical spin-symmetry-broken states. Moreover, the rotationally-invariant DFT+U methodology does not capture well the effect of the Hund's coupling J, which is known to be large in iron based systems. It was recently shown that the effect of strong correlations are not always driven by the Coulomb repulsion U alone, but in some cases act in combination with the Hund's coupling J [12–14]. Understanding the effect of strong correlations in heme, and in particular how the symmetry of the highest occupied molecular orbital (HOMO) is affected by U and J, is important in the context of describing the CO binding, which was shown to be strongly dependent on the HOMO symmetry [15].

Recent progress has been made in this direction by dynamical mean field theory [16] (DMFT), combined with DFT (DFT+DMFT) which can refine the description of the charge and spin of correlated ions, and describes in a remarkable way the strong correlations, induced by both U and J. Also, DFT can only describe a static magnetic moment associated with a spin symmetry broken state, and requires the inclusion of the spin-orbit interaction to explain a change of spin states [17]. This is not necessary at the DMFT level, which describes both static and fluctuating magnetic moments within the same framework.

In this work, we extend the DFT+U analysis by means of the combination of state-of-the-art linear scaling DFT [18] with DMFT, and apply this methodology to heme. The methodology builds upon our earlier works [19] and is described in detail in the supplementary material.

Although DFT+DMFT has been widely used to study solids, in this study we apply our real-space DFT+DMFT implementation to a moderately large molecule, extending the scope of applicability of DMFT to biology in an unprecedented manner. DMFT allows the quantum and thermal fluctuations, missing in zero-temperature DFT calculations, to be recovered. Moreover, it includes within the calculation both the Coulomb repulsion U and the Hund's coupling J. Which of U or J drives the many body effects in heme [14] remains an open question, paramount to understanding ligand bind-

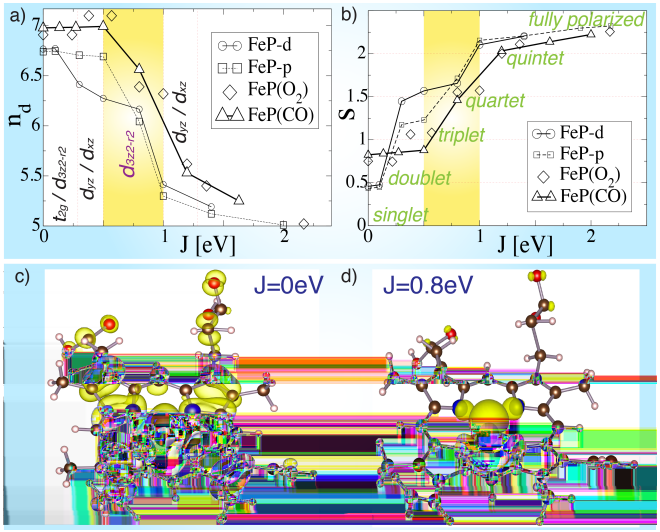

FIG. 1: **Orbital selection scenario:** Dependence of a) the iron $3d$ subspace occupancy n_d and b) the effective spin quantum number s on the Hund's coupling J, for both unligated and ligated heme models. The physically relevant region $0.5\text{ eV} < J < 1\text{ eV}$ is highlighted in yellow. Isosurfaces of the real-space representation of the electronic spectral density of the HOMO of FeP-d for c) $J = 0$ eV and d) $J = 0.8$ eV. The large central sphere shows the location of the iron atom, and the four blue spheres indicate nitrogen atoms.

ing, that we address in this work. Methods are available to obtain U and J parameters appropriate to DMFT [20], but in this work we focus on the dependence of the results with the Hund's coupling J, and we verify that our calculations are not sensitive to the Coulomb repulsion U or to the temperature T [21]. The key question that we address in this work is: to what extent does the Hund's coupling, so far neglected in all studies applied to heme, affect the binding of heme to O_2 and CO ligands, and in particular does J reduce the strong affinity for CO binding? If not specified otherwise, we use a similar value $U = 4$ eV to those previously computed for DFT+U [7], and ambient temperature $T = 294$K. The methodology is described in detail the supplementary material. Ionic geometries were obtained for four different configurations: unligated deoxyheme, FeP-d; the heme-CO complex carboxyheme, FeP(CO); the heme-O_2 complex oxyheme, FeP(O_2); and a theoretical planar version of deoxyheme, FeP-p.

We first discuss the dependence of the iron $3d$ subspace occupancy n_d on the Hund's coupling parameter J (Fig. 1.**a**). We emphasize that the expectation value of the occupancy n_d of the iron $3d$ sub-shell is not constrained to integer values in DFT and DFT+DMFT, since the iron occupation is a local observable, and hence does not commute with the Hamiltonian and is not conserved and there are valence fluctuations.

In the typical region of physically meaningful values of the Hund's coupling for iron $3d$ electrons, $J \approx 0.8$ eV, [22] we find a very sharp dependence of the electronic density on J. In fact, $J \approx 0.8$ eV places heme directly in the transition region between low-spin states and the $n_d = 5$ e fully-polarized state obtained for large Hund's coupling. We note that our results are weakly dependent on the choice of the Coulomb repulsion U (see sup. material).

In Fig. 1.**b**, we show the effective quantum spin number, which is associated to the norm of the angular spin vector $\mathbf{S}$ by the usual relation $|\mathbf{S}| = \sqrt{s(s+1)}$. The spin s shows characteristic plateaux as a function of the Hund's coupling at the semi-classically allowed values of the magnetization (corresponding to pure doublet, triplet, quartet, and quintet states). A fully-polarized state is recovered for sufficiently large Hund's coupling, as expected.

At $J = 0.8$ eV, and almost irrespective of ligation and doming, we find that heme has a spin expectation value of $s \approx 1.5$ corresponding to a quartet state in a semi-classical picture. Our results indicate that the true many-body wave-function of FeP-d is thus an entangled superposition of triplet and quintet states. The proposition that heme might be in an entangled state was pointed out early [23] in the context of a Pariser-Parr-Pople model Hamiltonian, and is confirmed by our DMFT calculations. In particular, this accounts for the striking differences obtained experimentally for very similar porphyrin systems, e.g. it was found that unligated FeP is a triplet [24] in the tetraphenylporphine configuration, a triplet with different orbital symmetry in the octaethylporphine configuration [25], and a quintet in the octamethyltetrabenzporphine configuration [26]. The strong dependence of the spin state with respect to small modifications in the structure is consistent with an entangled spin state.

In our calculations, we find that both oxyheme and carboxyheme adopt a low spin state for $J < 0.25$eV and larger multiplicities in the physical region of $J \approx 0.8$eV, while in both cases the spin state is very close in character to that of unligated deoxyheme. Significantly, we observe only subtle differences between FeP(O_2), FeP(CO) and FeP-d for $J = 0.8$ eV, while the DFT and DFT+U treatment yields ground-states for carboxyheme and oxyheme of pure closed-shell and open-shell singlet configurations, respectively [6, 7, 9].

Moreover, we find that the symmetry of the highest occupied molecular orbital (HOMO) of FeP-d, as estimated from the real-space spectral density of the prominent feature below the Fermi level, is highly dependent on the Hund's coupling J. In particular, for $J = 0$ eV, the HOMO is an admixture of orbital characters (see vertical labels in Fig. 1.**a**). However, the Hund's coupling drives a rather complex orbital selection, such that for the region of greatest interest, $J \approx 0.8$ eV, the HOMO predominantly exhibits $d_{3z^2-r^2}$ symmetry. The orbital selection process also induces a pinning of the Fermi density to the quantum impurity, such that it is delocalized for $J = 0$ eV (see Fig. 1.**c**), while for $J = 0.8$ eV (Fig. 1.**d**) it is instead localized to the iron $3d$ sub-shell.

In our view, this relates to the Fe-O-O angle obtained

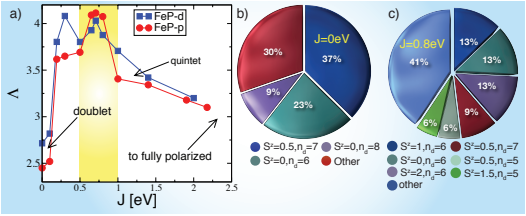

FIG. 2: **Valence fluctuations:** a) Von Neumann entropy Λ obtained by DFT+DMFT for FeP-p (circles) and FeP-d (squares). Histograms of the dominant electronic configurations for FeP-d for b) $J = 0$ eV and (c) $J = 0.8$ eV. The pie wedge labelled *other* contains configurations with a weight smaller than 3%. The iron $3d$ spin S^z and iron $3d$ occupancy n_d of the dominant configurations is indicated.

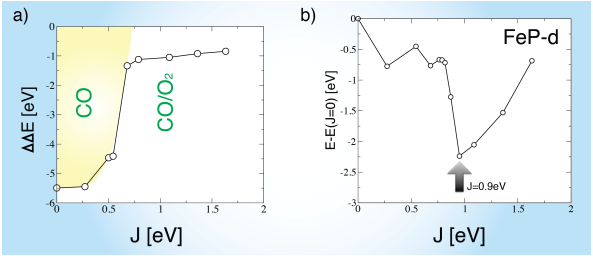

FIG. 3: **Energetics:** a) Difference in CO and O_2 binding energies $\Delta\Delta E$. The binding to CO is always favored, however the imbalance is strongly reduced for $J > 0.5$eV. b) Total energy of FeP as a function of J. The minimum of the total energy is obtained for $J = 0.9$eV.

in FeP(O_2) [27]. Indeed, the bent geometry of FeP(O_2) can be explained by a favorable interaction between the p*-orbital of the O_2 and the $d_{3z^2-r^2}$ -orbital on Fe [27]: the O_2 p*-orbital is closer in energy to $d_{3z^2-r^2}$ compared to the p*-orbitals in CO, and hence it gains more energy by bending, which increases the overlap. For FeP(CO) the situation is opposite, and there is no stabilization gained by bending [27]. On the contrary, the bending in FeP(CO) is induced by the strain of the protein and it reduces the binding energy. Naively, the orbital selection of the $d_{3z^2-r^2}$ orbital is hence expected to go in the direction of curing the strong O_2 and CO imbalance. Moreover, the charge localization at the Fermi level suggests that other artificial binding between the non-metallic atomic orbitals of heme and strong electronegative O_2 will not be obtained, and hence will protect heme from undesired charge transfer.

We now discuss the degree of quantum entanglement exhibited by FeP-d and FeP-p (see Fig. 2.**a**). We computed the von Neumann entropy $\Lambda = -\mathrm{tr}\,(\hat{\rho}_d \log(\hat{\rho}_d))$, where $\hat{\rho}_d$ is the reduced finite-temperature density-matrix of the iron $3d$ impurity subspace, traced over the states of the AIM bath environment. The entropy quantifies to what extent the wave-function consists of an entangled superposition.

We observe that the entropy rises sharply at $J \approx 0.25$ eV, corresponding to the transition from the doublet spin state to the triplet/quintet entangled state. As expected, the entropy is small in the low-spin region ($J < 0.25$ eV) and also in the fully-polarized limit. At $J = 0$ eV (Fig. 2.**b**), we find that the dominant configuration consists of the doublets $(d_{3z^2-r^2})^2(d_{xy})^2(d_{xz})^2$, with a single electron in the $d_{x^2-y^2}$ orbital. The latter hybridizes strongly with the nitrogen $2p$ orbitals, but all other orbitals are mostly filled or empty, so this configuration is, essentially, a classical state with a finite magnetic moment.

At larger J values, however, such as $J = 0.8$eV (Fig. 2.**c**), all orbitals are partially filled, and an increasing number of electronic configurations, with different valence and spin, contribute to the statistics, and thus the iron impurity wave-function is *fluctuating*. Although the valence fluctuation are captured to some extent at the DFT level ($\Lambda_{DFT} \approx 0.75$), we find that many body effects contribute significantly to the entropy.

Our results indicate that as FeP-d and FeP-p molecules approach a regime with large entanglement for $J \approx 0.5$, with a concomitant orbital selection close to the Fermi level. The orbital selection close to the Fermi level in turn induces a charge-localization effect. The latter effect of the Hund's coupling can be understood with a simple picture: a large Hund's coupling partially empties the $d_{3z^2-r^2}$ orbital and brings the weight of this orbital closer to the Fermi level, thereby reducing the hybridization between the iron $3d$ states and the nitrogen $2p$ states close to the Fermi level. The subtle interplay between the charge-localization induced by the Hund's coupling (orbital selection close to the Fermi energy) and the delocalization induced by strong correlations (the tendency for electrons to escape the iron $3d$ orbitals in order to reduce the Coulomb energy) is captured by the DFT+DMFT methodology but is absent in Kohn-Sham DFT. We emphasize that these ingredients are paramount to an estimation of the charge transfer and binding properties between the iron atom and the ligand in oxyheme and carboxyheme.

Let us next discuss the effect of the Hund's coupling with respect to the unrealistic imbalance between the binding energies of CO and O_2 obtained by DFT. The binding energy is defined as: $\Delta E = E(FeP(X)) - (E(FeP) + E(X))$, where X=CO or X=$O_2$. The difference between the binding energies $\Delta E(CO) - \Delta E(O_2)$ is obtained by: $\Delta\Delta E = \Delta E_{CO} - \Delta E_{O_2}$. For $J = 0$eV, we find that the binding to CO is dramatically favoured, when compared to the binding to O_2 (Fig. 3.**a**): the difference in binding energies is of the order of 5eV. Although the binding to CO is favoured for all values of J, we find that it is dramatically improved for $J > 0.5$eV, and is reduced down to 1eV. This suggests that other effects might be important to reduce further the CO/O_2 imbalance, such as that the effect of the protein via the bending of the Fe-C-O angle [9].

It is also worth noting that we find that the total energy of the molecule is minimized for $J = 0.9$eV

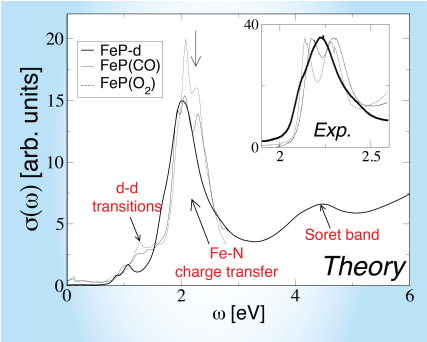

FIG. 4: **Optical measurements:** Optical conductivity of FeP-d (bold line) and FeP(CO) (solid) and FeP(O_2) (dashed line). The vertical arrow indicates the energy of the experimental peak associated to the Fe-N charge transfer. Inset: experimental measurements [28] for unligated heme (bold line), oxy- (dashed line) and carboxy- (solid) heme are shown for comparison. $J = 0.8$eV was used for all calculations above.

(Fig. 3.**b**), suggesting further that the heme molecule is particularly well suited to host metallic d atoms, which tend to have a large screened J interaction when hybridising to light elements such as nitrogen or oxygen.

We now move to our calculations of the optical absorption spectra of heme (Fig. 4). Our theoretical absorption spectra, shown in Fig. 4, are in reasonable agreement with experimental data [28], in particular for the optical transitions at $\omega \approx 2$ eV. We attribute this spectral feature to charge-transfer excitations from iron to nitrogen-centered orbitals. The spectrum is dominated by the characteristic porphyrin Q-bands (those at ≈ 2eV), and Soret bands [29] (at ≈ 4eV). Our results offer insight into the infrared absorption band present at ≈ 1eV, in our calculation, and observed in experiments at 0.6 eV [30]. This infrared peak is described, in our calculations, as arising from transitions between the $d_{3z^2-r^2}$ spectral feature (HOMO) below the Fermi level and the LUMO (quasi-degenerate d_{xz} and d_{yz}) above the Fermi level.

Interestingly, we find that the infrared optical weight in unligated heme, associated with *d-d* transitions and present in FeP-d, is absent in the planar theoretical model FeP-p. Hence, the symmetry breaking associated with the doming effect of the iron-intercalated porphyrin macrocycle permits *d-d* optical transitions, and is responsible for the spectral weight in the infrared regime. We note that experimental spectra for FeP(CO) and FeP(O_2) exhibit a double peak structure at $\omega \approx 2$eV, absent from our calculations done at $J = 0$eV, but recovered for $J > 0.8$eV. The best agreement with the experimental data is obtained for $J = 0.9$eV. Finally, we extended our calculations to the time dependence of the magnetization of the iron atom after an initial quench in polarization (see sup. material). We propose that time-resolved spectroscopy may be used as a sensitive probe for the ligation state of heme.

In conclusion, we have carried out linear-scaling first-principles calculations, in combination with DMFT, on both unligated and ligated heme. We have presented a newly-developed methodology applied to a molecule of important biological function, exemplifying how subtle quantum effects can be captured by our methodology. In particular, we have found that the Hund's coupling J drives an orbital selection process in unligated heme, which enhances the bonding in the out-of-plane direction. The von Neumann entropy quantifying valence fluctuations in the iron $3d$ subspace is large for the physical values of $J \approx 0.8$eV. This scenario sheds some light on the strong CO and O_2 binding imbalance problem obtained by extracting the binding energies in simpler zero temperature and $J = 0$eV DFT calculations. The difference in binding energies is dramatically reduced for physical value of $J \approx 0.8$. The smaller remaining imbalance might be further explained by the strain energy contained in the protein structure [9] or by the contribution from the entropic term. Finally, the relevance of a finite Hund's coupling in heme is confirmed by the total energy extracted from the DFT+DMFT of unligated heme, which shows a minima for $J = 0.9$eV.

We have proposed a new mechanism for ligand binding to heme based on an orbital selective process, on this basis, a scenario which we term *bonding determined by local valence fluctuations*. Finally, we have obtained a reasonable agreement between experimental and our theoretical optical absorption spectra, our description accounting for the observation of optical transitions in the infrared regime and the double peaked structure of the optical response at $\omega \approx 2$eV.

At the time of writing, we became aware of related application of DMFT to an organometallic crystal [31].

We are grateful to R.H. McKenzie for comments and bringing Ref. [23] to our attention, and to D. Cole for many insightful discussions. C.W. was supported by the Swiss National Foundation for Science (SNFS). D.D.O'R. was supported by EPSRC. N.D.M.H was supported by EPSRC grant number EP/G055882/1. P.B.L is supported by the US Department of Energy under FWP 70069. Calculations were performed on the Cambridge High Performance Computing Service under EPSRC grant EP/F032773/1. Correspondence and requests for materials should be addressed to C.W.

[1] A. M. P. Sena, et al. *Phys. Rev. B*, 79(24):245404, 2009.
[2] D. D. O'Regan, et al. *Phys. Rev. B*, 82:081102, 2010.
[3] P. M. Oppeneer, et al. *Progress in Surface Science*, 84(1-2):18, 2009.
[4] W. Kohn et al. *ibid.*, 140:A1133, 1965.
[5] D. Benito-Garagorri, et al. *Dalton Trans.*, 40:4778, 2011.
[6] C. Rovira, et al. *Chem. Phys. Lett.*, 271:247, 1997.
[7] D. A. Scherlis, et al. *J. Phys. Chem. B*, 111:7384, 2007.
[8] H. J. Kulik, et al. *Phys. Rev. Lett.*, 97:103001, 2006.
[9] D. J. Cole, et al. *J. Phys. Chem. Lett.*, 3:1448, 2012.

[10] C. Rovira et al. *Chem. A Eur. J.*, 5(1):250, 1999.
[11] P. M. Panchmatia, et al. *J. Phys. Chem. A*, 114:13381, 2010.
[12] Z. P. Yin, et al. *Nat Phys*, 7(4):294, 2011.
[13] L. de' Medici. *Phys. Rev. B*, 83:205112, 2011.
[14] L. de' Medici, et al. *Phys. Rev. Lett.*, 107:256401, 2011.
[15] G. Kresse, et al. *Phys. Rev. B*, 68:073401, 2003.
[16] A. Georges, et al. *Rev. Mod. Phys.*, 68:13, 1996.
[17] H. Nakashima, et al. *J. Comput. Chem.*, 27:426, 2006.
[18] C.-K. Skylaris, et al. *Phys. Rev. B*, 66:035119, 2002.
[19] C. Weber, et al. *Phys. Rev. Lett.*, 108:256402, 2012.
[20] L. Vaugier, et al. 2012.
[21] See Supplemental Material at http://link.aps.org /supplemental /10.1103 /PhysRevLett .000.000000 for the methodology and additional data.
[22] A. Kutepov, et al. *Phys. Rev. B*, 82:045105, 2010.
[23] D. A. Case, et al. *Journal of the American Chemical Society*, 101(16):4433, 1979.
[24] G. Lang, et al. *J. Chem. Phys.*, 69:5424, 1978.
[25] J. P. Collman, et al. *J. Am. Chem. Soc.*, 97:2676, 1975.
[26] J. R. Sams et al. *Chem. Phys. Lett.*, 25:599, 1974.
[27] D. T. R. Hoffmann, M.M.-L. Chen. *Inorg. Chem.*, 16:503, 1977.
[28] J. M. Steinke et al. *Clin. Chem.*, 38(7):1360, 1992.
[29] R. Schweitzer-Stenner, et al. *J. Chem. Phys.*, 127(13):135103, 2007.
[30] M. D. Kamen, et al. *Proc. Nat. Acad. Sci.*, 70(6):1851, 1973.
[31] J. Ferber, et al. *arXiv/1209.4466.*